Automatic dissociation between microvasculature and larger vessels for Ultrasound Contrast Imaging

Antonios Perperidis -*IEEE Member*, David Thomas, Michalakis Averkiou, Colin Duncan, Alan McNeilly, Mairead Butler, Vassilis Sboros

***Abstract*—Microvasculature density (MVD) provides an established biomarker for the prognosis of numerous diseases associated with abnormal microvascular networks. The accurate, robust and timely assessment of MVD changes facilitates disease detection, treatment monitoring and patient stratification. Nevertheless, the current gold standard (PET) for MVD quantification is not used in clinical practice due to its high costs and potential health hazards. Contrast Enhanced Ultrasound (CEUS) imaging can provide an attractive alternative. However, the limited dissociation between larger vessels and microvasculature in the imaged tissues limits the accuracy and robustness of CEUS. This study proposed a novel, and fully automatic technique that dissociates larger vessels from microvasculature in CEUS imaged tissues. The ovine Corpus Luteum (CL) was used as an in vivo model for the development and assessment of the proposed technique.**

I. Introduction

Microvascular density (MVD) relates to tumour angiogenic potential and is an established biomarker for the prognosis of disparate cancers as well as of other diseases associated with abnormal microvascular networks (i.e. ischaemia and inflammatory disease). A number of anti-angiogenic therapies that target these cancers are currently under development. An important aim of medical imaging research is, therefore, to provide a robust, in vivo, longitudinal assessment of MVD that facilitates (i) disease detection, (ii) treatment monitoring, (iii) ongoing evaluation of response criteria, and (iv) informed management paradigms. The current response evaluation criteria for solid tumours (RECIST) utilises Computerised Tomography (CT) to assess tumour volume changes at least three months after the treatment. Such indirect assessment significantly limits early personalisation based on treatment response and may contribute to suboptimal morbidity and mortality rates. Though desirable, it is currently difficult to assess microvascular (MV) perfusion using any state of the art imaging technology. The gold standard, and only commercially available tool, is Positron Emission Tomography (PET) [1]. However, quantitative perfusion measurement using PET is expensive, hazardous, of limited availability and thus difficult to use routinely in clinical practice, especially in large populations.

Ultrasound imaging is a safe, low cost and widely accessible technology. Furthermore, sub-capillary sized microbubbles (MBs) that are thin-shelled and gas-filled, unlike most contrast agents from other imaging modalities, behave kinetically like red blood cells and do not extravasate. They can therefore be used along with modern ultrasound systems, in a process known as Contrast Enhanced Ultrasound (CEUS) imaging, to image and quantify microvascular blood flow and volume providing a live and longitudinal in vivo assessment of MVD [2, 3]. CEUS has recently been introduced in clinical cardiology and liver radiology [4-6], assessing microvasculature related pathology. However, the quantification of perfusion is not fully developed and, thus, not used in the clinic. The current gold standard for such measurement, PET with (with $H_2{}^{15}O$), has shown 9% intra-subject variability. In comparison, CEUS has provided 32% variability [1]. A major contributor to the limited accuracy of CEUS is the lack of accurate information derived solely from capillary flow and volume, required to determine tissue perfusion [6].

Vessels larger than capillaries (VLC) form a significant part of CEUS image data, impeding accurate microflow measurements. More precisely, VLCs can (i) supply non-neighbouring regions of the tissue, hence VLC flow may contain no physiological information on the state of the tissue in the imaged region of interest (ROI), and (ii) directly supply local microvasculature, yielding indirect diagnostic information on microflow [6]. However, pulsatility, flow resistance indices, or flow to area ratios using Doppler data from larger vessels do not actually represent the vascularity or vascularisation of the imaged tissue [7]. There is a real opportunity to establish CEUS as the leading modality for perfusion assessment in the clinic by improving measurement uncertainty to levels similar to that of PET. In order to achieve this, the separation of microvasculature from larger vessels is crucial. Currently, a technique using Colour Doppler information to highlight larger vessels, and then manually segment a ROI excluding the identified VLCs, is employed. This technique is elaborate, cumbersome and highly subjective. The overarching aim is to generate software that automatically, accurately and reproducibly dissociates between signals from VLCs and signals from capillaries in order to increase the accuracy and precision of quantification of microvascular flow and volume with CEUS.

Research supported by the British Heart Foundation (PG/10/021/28254).

A. Perperidis is with the Institute of Biological Chemistry, Biophysics and Bioengineering (IB3), Heriot Watt (HW) University, Edinburgh, UK (corresponding author, e-mail: A.Perperidis@hw.ac.uk).

D. H. Thomas was with the University of Edinburgh and is now with the Department of Radiation Oncology, UCLA, Los Angeles, CA, USA (e-mail: dhthomas@mednet.ucla.edu).

M. Averkiou is with the Department of Mechanical Engineering, University of Cyprus, Nicosia, Cyprus (email: maverk@ucy.ac.cy).

W. C. Duncan is with the MRC Centre for Reproductive Health (CRH), University of Edinburgh (UofEd), Edinburgh, UK (e-mail: W.C.Duncan@ed.ac.uk).

A. S. McNeilly is with the CRH, UofEd (e-mail: A.McNeilly@ed.ac.uk).

M. Butler is with the IB3, HW University (e-mail: M.Butler@hw.ac.uk).

V. Sboros is with the IB3, HW University (e-mail: V.Sboros@hw.ac.uk).

A number of kinetics models have been proposed for destruction replenishment or bolus studies [8]. The developing ovine corpus luteum (CL) is highly angiogenic and predictably develops a tumor-like microvascular network of around 1cm diameter that exists for approximately 10 days before it routinely regresses [9]. In addition, complete CL vascular regression can be pharmacologically induced with Prostaglandin F (PGF) within 24h [9]. Consequently, this study utilised the ovine CL as a dynamic, regulated and predictable capillary bed that facilitated the modelling of microvascular flow to develop and assess imaging technology for detecting small perfusion changes in vivo.

II. Methods

A. Animal and Imaging Methodology

All data were acquired from an adult ewe under terminal general anaesthesia with project licence approval from the Home Office (McNeilly PPL 60/3906). The ewe's ovaries were exposed by laparotomy and stabilised to avoid interfering with the ovarian blood supply. This enabled the ultrasound probe to be positioned and oriented for optimal data acquisition. Heart rate and blood pressure were monitored and recorded throughout the experiment.

Eight sets of B-mode and CEUS datasets (Fig. 1) were acquired using a Philips iU22 ultrasound scanner (Philips Medical Systems, Bothell, WA, USA) along with a high frequency linear array L12-5 operating on a contrast imaging mode (nonlinear pulsing schemes). A 2.4ml bolus of Sonovue® (Bracco, Geneva, Switzerland) was utilised to highlight the tissue perfusion of the CL. All scans were performed across the largest cross section of the CL including the ovarian artery. Data were stored in DICOM format for offline analysis. At the end of the study the ovary was removed and fixed for immune histological analysis (Fig. 3.a) of the VLCs (smooth muscle actin) and capillary density (lectin) for direct comparison with the ultrasonic image data.

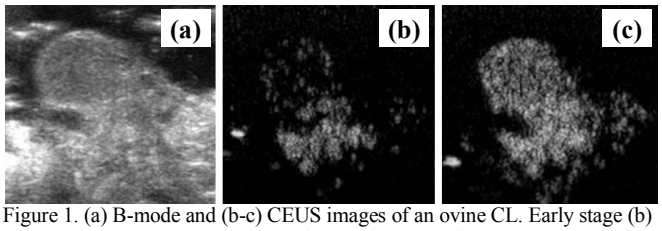

Figure 1. (a) B-mode and (b-c) CEUS images of an ovine CL. Early stage (b) and peak stage (c) of the CL perfusion illustrated.

B. Spatial Alignment of CEUS Frame Sequences

In order to correct for on-plane movements of the imaged structure during the multi-frame data acquisition, each frame within the processed frame sequence was spatially aligned to a reference frame. The movements were mostly due to respiratory motion, hence the reference frame was manually selected at the end-expiratory phase. Off-plane movements of the imaged CL, such as probe slippage, were kept to a minimum during data acquisition.

The data alignment was initially performed on the B-mode images employing an intrinsic, image based, rigid registration approach [10], which sufficiently compensated for CL displacement during the multi-cycle data acquisition. The Nelder-Mead's simplex optimisation strategy was utilised in order to derive the optimal transformation maximising the Normalised Cross Correlation (NXC) between the registered images [11]. Nelder and Mead's simplex provided a good trade-off between robustness and convergence time [12], while NXC provided an accurate, robust and efficient approach when compared to other image similarity measures. To further enhance the accuracy and robustness of the proposed approach, outliers in the spatial transformation over consecutive frames were identified and removed. Due to the smooth, periodic nature of the respiratory movement, smoothing splines were employed to compensate for sharp, irregular transformations across a B-mode frame sequence. The splines were customised to not smooth over local extrema in the processed transformation curve (end-expiratory and end-inspiratory phases). Having identified the transformation required to align each frame in the B-mode sequence to the reference frame, the transformations were then applied to align the corresponding CEUS images.

C. Time Intensity Curves (TICs) and Parametric Mapping

In order to extract a location specific collection of TICs that characterised the entire CL, a 2D rectangular grid was laid over the scanning plane of the multi-frame CEUS data. For each cell of the grid, a TIC was generated. A 2x2 pixel grid compensated for small misalignment errors during the spatial registration of the frame sequence without sacrificing much of the spatial resolution of the processed data. For each of the extracted TICs, a smoothing spline compensated for the high levels of noise present in the original curve. A Log-normal curve (*LN*) was then automatically fitted to the smoothed TIC [8].

$$LN = \frac{1}{S * \sqrt{2\pi} * x} * e^{-(\ln(x) - M)^2 / 2 * S^2} \quad (1)$$

where M and S are the mean and standard deviation of the TIC. Fig. 2 illustrates a typical example of the original, smoothed and Log-normal fitted TICs. Log-norm curves that fitted poorly (R^2<80%) to the corresponding smoothed curves were discarded.

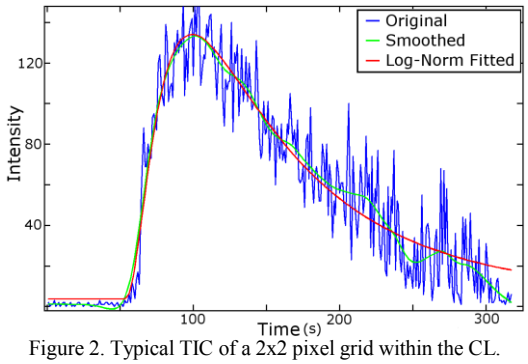

Figure 2. Typical TIC of a 2x2 pixel grid within the CL.

The shape and size of a TIC contains valuable information on the size of the underlying vasculature. Consequently, the Log-normal model was employed to derive, a number of parameters characterising each TIC, including: the peak intensity value (IP), the mean transit time (MTT), the wash-in-rate (WIR), the wash-out-rate (WOR), the full width at half maximum (FWHM) and the area under the curve (AUC) [8]. A parametric (probabilistic) image was created for each of the six TIC parameters with the intensity

value of each pixel representing the probability of the underlying structure to be a larger vessel. Given the assumption that the larger the vessel size, the larger value of each utilised parameter, the intensity values were derived using a linear mapping between the minimum and maximum value of the corresponding parameter.

Some of the parametric images exhibited larger variance between different regions of the CL than others. Larger variance may translate to more information on the nature of the underlying structures. On the other hand, some parametric images displayed highly correlated information. Principal Component Analysis (PCA) [13] was therefore used on the information from the 6 parametric images deriving a new set of uncorrelated (independent) variables. The first three principal components represented more than 98% of the variance (information) within the 8 parametric images. The first principal component (PC1) (Fig.3.c) accounted for any structure distinguishable in the 6 parametric images (>80% of variance) while PC2 and PC3 contained mostly noise.

D. Large Vessel Dissociation

PC1, containing most information on underlining imaged CL, was further processed to identify larger vessels and dissociate them from microvasculature. PC1 was subsequently converted into a 3D map, with the Z-axis representing intensity information (Fig. 3.d). The mean curvature C [14] was derived for each pixel within the map.

$$C = \frac{E * N + G * L - 2 * F * M}{2 * (E * G - F^2)} \quad (2)$$

where E, F and G were the 1st fundamental coefficients while L, M and N were the 2nd fundamental coefficients of the surface $\Phi \subset R^3$. Peaks, ridges and saddles (positive curvature) corresponded to larger vessels feeding the surrounding microvasculature, which in turn was represented by valleys (negative curvature). Consequently, the mean curvature on the 3D surface enabled the automatic dissociation between larger vessels and microvasculature without the use of a hard intensity threshold.

III. Results and Discussion

Fig. 3.a illustrates an example histological slice of the imaged CL while Fig. 3.b and 3.f illustrate the corresponding regions (binary masks) identified as VLCs by using Colour Doppler information and the proposed automatic technique respectively. While the imaging plane between the histology and the ultrasound data is most likely not identical, similar patterns can be recognised across the CL. For example, large VLCs circulate the blood on the perimeter of the CL. Then, a set of axial VLCs distribute the blood from the perimeter towards the centre of the CL which in turn feed a network of VLCs throughout the entire CL. Fig.3.g overlays the binary masks from Fig. 3.b and 3.f. The high level of similarity between the binary masks extracted using the automatic and the Colour Doppler approach is evident. In fact 75% of the automatically identified larger vessels overlap with the corresponding Doppler identified areas, mostly in the CL periphery. However, the proposed automatic technique appears to provide higher level of detail (25% non-overlap) mostly at the centre of the CL, on what is perceived as "larger vessels". In addition, colour bleeding in the Doppler binary masks results in the misclassification of peripheral microvasculature near as VLCs. Doppler uses 175% more pixels to classify the same region around the circumference of the CL when compared to the proposed parametric approach. These misclassifications by Colour Doppler can have a direct degrading effect in the accuracy and precision of tissue perfusion quantification.

Fig. 4.a illustrates an example of 7 regions of interest (ROIs), all manually classified (by expert) as VLCs by employing Doppler binary masks. However, their corresponding TICs, as plotted in Fig. 4.a and 4.b, demonstrate very different characteristics. In fact, the ROIs correspond to areas identified as arteries (1), veins (1), large vessels (3) and microvasculature (2). Microvasculature has been purposely selected in close proximity to the VLCs to highlight the sensitivity of the proposed dissociation technique. As expected, there is a clear distinction in peak value, width and area between the TICs corresponding to larger vessels and TICs corresponding to microvasculature. Moreover, as illustrated in Fig. 4.b, contrast arrives in arteries first, followed by larger vessels that distribute the blood in the microvasculature and is finally transferred out of the CL through the veins. Fig. 4.c and 4.d. provide further TIC examples from 7 ROIs identified by the proposed automatic approach as VLCs and 7 ROIs identified as MV. Both the VLC and microvasculature examples were carefully distributed across the entire CL, with some microvasculature in very close proximity to nearby VLCs. This level of detail cannot be achieved by the current manual dissociation approach utilising Colour Doppler information. The proposed multi-parameter approach, taking into consideration such information from the TICs, correctly dissociates between the larger vessels and microvasculature in close proximity without the need for an objective measurement of flow.

TABLE I. TIC Parameter Range Across 14 ROIs

	MVs (7)		VLCs (7)	
	Mean	**RSTD (%)**	**Mean**	**RSTD (%)**
IP	88.69	6.21	113.14	14.42
MTT	152.63	17.59	200.16	19.74
WIR	2.07	13.53	2.65	18.87
WOR	0.54	18.51	0.55	20.00
FWHM	127.43	12.74	151.29	10.91
AUC	14221.00	14.34	22666.00	17.55

Table I summarises the parameter range (Mean and Relative Standard Deviation - RSTD) extracted from the VLC and MV TICs respectively. All but the WOR provide valuable information in the automatic dissociation process. The proposed multi-parameter technique, combined with PCA, increases the accuracy and robustness of large vessel identification and therefore provides a powerful pre-processing tool in the perfusion measurement related to the underlying microvasculature. Finally, the large variability observed in VLC TICs is attributed to the large size disparity of VLCs, ranging from (i) arteries and veins, to (ii) intermediate VLCs distributing the blood to (iii) smaller arterioles and venules that connect directly to local capillary beds (MV). As demonstrated by Fig. 4 and Table I, the parametric images provide valuable information that can be utilised for further classification amongst these VLCs.

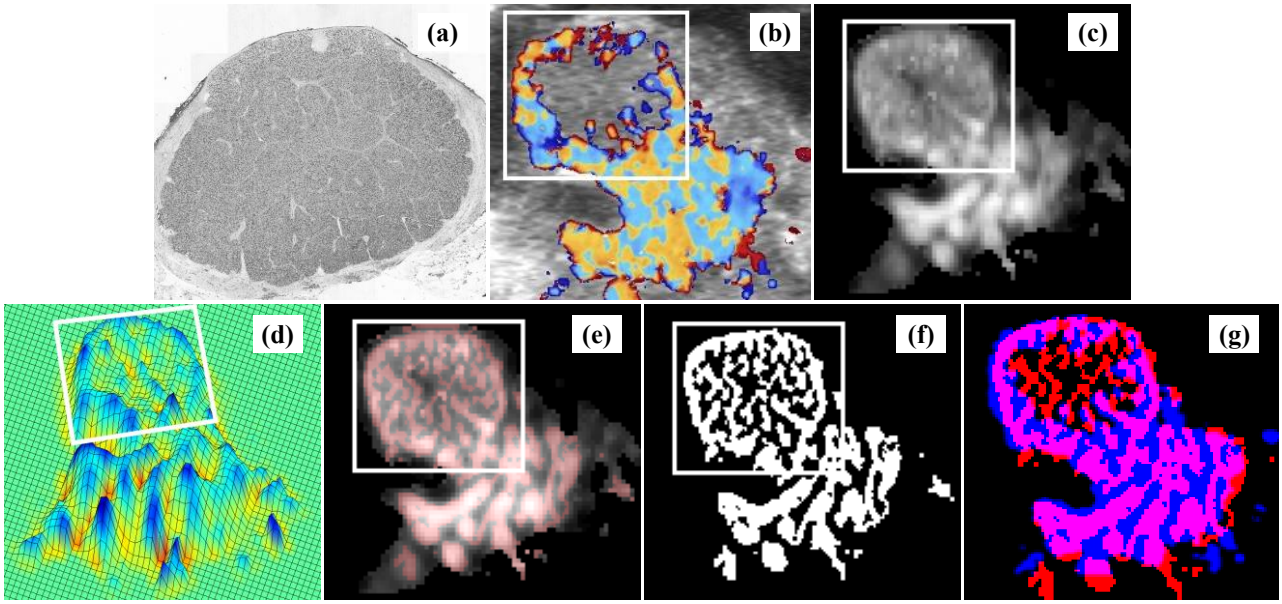

Figure 3. (a) Histological slice of CL, (b) Colour Doppler highlighting VLCs, (c) PC1 from parametric imaging, (d) 3D representation of PC1 used to derive curvature, (e) VLCs over PC1, (f) corresponding VLC binary mask and (g) overlay of Colour Doppler and parametric binary masks. ROI approx. 10mm.

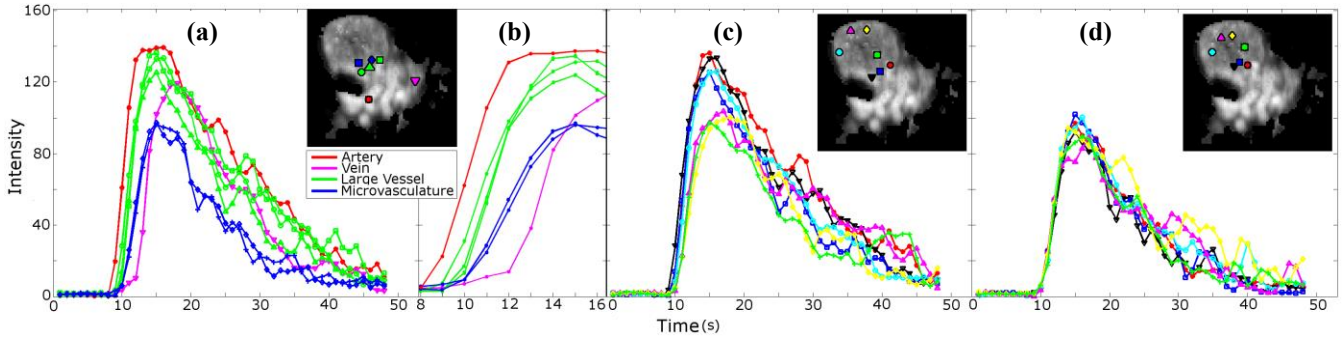

Figure 4. (a-b) 7 ROIs and corresponding TICs representing arteries (1), veins (1), large vessels (3) and microvasculature (2), (c) 7 ROIs and corresponding TICs representing a range of VLCs across the entire CL, (d) 7 ROIs and corresponding TICs representing a range of MVs across the entire CL.

IV. Conclusion

This study introduced a novel and fully automatic approach for the dissociation between vessels larger than capillaries and microvasculature in CEUS image sequences. The proposed technique utilised a set of parametric images derived from localized TICs and thus required no direct measurement of flow. It also demonstrated potential for a more accurate and robust dissociation between VLCs and microvasculature than the current laborious and highly subjective approaches using Colour Doppler. Such dissociation could enable a much needed increase in accuracy and precision in the quantification of tissue perfusion.

References

[1] P.A. Dijkmans, P. Knaapen, G.T.J. Sieswerda, E. Aiazian, C.A. Visser, A.A. Lammertsma, F.C. Visser, O. Kamp, "Quantification of Myocardial Perfusion Using Intravenous Myocardial Contrast Echocardiography in Healthy Volunteers: Comparison with Positron Emission Tomography." *Journal of the American Society of Echocardiography*, vol. 19, no. 3, pp. 285-293, Mar. 2006.

[2] C.F. Dietrich, M.A. Averkiou, J.M. Correas, N. Lassau, E. Leen, F. Piscaglia, "An EFSUMB introduction into Dynamic Contrast-Enhanced Ultrasound (DCE-US) for quantification of tumour perfusion." *Ultraschall in Med*, vol. 33, no. 4, pp. 344-351, 2012.

[3] E. Leen, M. Averkiou, M. Arditi, P. Burns, D. Bokor, T. Gauthier, Y. Kono, O. Lucidarme, "Dynamic contrast enhanced ultrasound assessment of the vascular effects of novel therapeutics in early stage trials." *European radiology*, vol. 22, no. 7, pp. 1442-1450, 2012.

[4] E. Quaia, "Microbubble ultrasound contrast agents: an update." *European Radiology*, vol. 17, no. 8, pp. 1995-2008, 2007.

[5] B.A. Kaufmann, K. Wei, J.R. Lindner, "Contrast Echocardiography." *Current Problems in Cardiology*, vol. 32, no. 2, pp. 51-96, Feb. 2007.

[6] V. Sboros, M.X. Tang, "The assessment of microvascular flow and tissue perfusion using ultrasound imaging." *Proceedings of the Institution of Mechanical Engineers. Part H, Journal of engineering in medicine*, vol. 224, no. 2, pp. 273-290, 2009.

[7] T. Miyazaki, M. Tanaka, K. Miyakoshi, K. Minegishi, K. Kasai, Y. Yoshimura, "Power and colour Doppler ultrasonography for the evaluation of the vasculature of the human corpus luteum." *Human Reproduction*, vol. 13, no. 10, pp. 2836-2841, 1998.

[8] C. Strouthos, M. Lampaskis, V. Sboros, A. Mcneilly, M. Averkiou, "Indicator dilution models for the quantification of microvascular blood flow with bolus administration of ultrasound contrast agents." *IEEE Transactions on Ultrasonics, Ferroelectrics and Frequency Control*, vol. 57, no. 6, pp.1296-1310, June 2010.

[9] V. Sboros, M. Averkiou, M. Lampaskis, D.H. Thomas, N. Silva, C. Strouthos, J. Docherty, A. Mcneilly, "Imaging of the ovine corpus luteum microcirculation with contrast ultrasound." *Ultrasound in Medicine & Biology*, vol. 37, no. 1, pp. 59-68, 2011

[10] L.G. Brown, "A survey of image registration techniques." *ACM Computing Surveys*, vol. 24, no. 4, pp. 325-376, 1992.

[11] J.P. Lewis, "Fast Template Matching." *Vision Interface*, vol. 95, no. 120123, pp. 15-19, 1995.

[12] J.A. Nelder, R. Mead, "A simplex method for function minimization." *The Computer Journal*, vol. 7, no. 4, pp. 308-313, 1965.

[13] I.T. Jolliffe, Principal Component Analysis, 2nd ed. Springer, 2002.

[14] A. Gray, *Modern Differential Geometry of Curves and Surfaces with Mathematica*, 2nd ed. Boca Raton, FL: CRC Press, 1977, pp. 373-380.